THE JOURNAL OF BIOLOGICAL CHEMISTRY VOL. 283, NO. 9, pp. 5577–5588, February 29, 2008

Structural Determinants of Calmodulin Binding to the Intracellular C-terminal Domain of the Metabotropic Glutamate Receptor 7A*[S]

Received for publication, November 20, 2007 Published, JBC Papers in Press, December 18, 2007, DOI 10.1074/jbc.M709505200

Astrid Scheschonka[‡], Stuart Findlow[§], Rudolf Schemm[‡1], Oussama El Far[‡2], John H. Caldwell[‡3], Matthew P. Crump[§4], Kate Holden-Dye[§], Vincent O'Connor[§], Heinrich Betz[‡5], and Jörn M. Werner[§6]

From the [‡]Department of Neurochemistry, Max Planck Institute for Brain Research, 60528 Frankfurt, Germany and the [§]School of Biological Sciences, University of Southampton, Southampton S016 7PX, United Kingdom

Calmodulin (CaM) binds in a Ca^{2+}-dependent manner to the intracellular C-terminal domains of most group III metabotropic glutamate receptors (mGluRs). Here we combined mutational and biophysical approaches to define the structural basis of CaM binding to mGluR 7A. Ca^{2+}/CaM was found to interact with mGluR 7A primarily via its C-lobe at a 1:1 CaM:C-tail stoichiometry. Pulldown experiments with mutant CaM and mGluR 7A C-tail constructs and high resolution NMR with peptides corresponding to the CaM binding region of mGluR 7A allowed us to define hydrophobic and ionic interactions required for Ca^{2+}/CaM binding and identified a 1-8-14 CaM-binding motif. The Ca^{2+}/CaM·mGluR 7A peptide complex displays a classical wraparound structure that closely resembles that formed by Ca^{2+}/CaM upon binding to smooth muscle myosin light chain kinase. Our data provide insight into how Ca^{2+}/CaM regulates group III mGluR signaling via competition with intracellular proteins for receptor-binding sites.

G-protein-coupled metabotropic glutamate receptors (mGluRs)[7] have been implicated in the regulation of transmitter release, short and long term modulation of synaptic transmission, neuronal development, and synaptic plasticity (1–4). mGluRs are structurally distinct from family A and B G-protein coupled receptors, as they possess a large extracellular ligand binding domain and a comparatively long intracellular C terminus (3, 5). At least eight different mGluR isoforms have been identified and classified into three subgroups based on sequence homology, downstream effectors, and agonist specificity. Group III mGluRs (mGluR 4 and 6–8) are specifically activated by L-amino(+)-2-amino-4-phosphonobutyric acid, negatively coupled to adenylate cyclase and, apart from mGluR 6, are exclusively located presynaptically. Coupling to other signal transduction pathways may occur in some tissues; for mGluR 7, inhibition of P/Q-type calcium channels involving phospholipase C has been demonstrated in cerebellar granule cells (6). With the exception of mGluR 6, which is exclusively found in the retina, group III mGluRs are expressed throughout the brain. The most abundant family member, mGluR 7, displays a low affinity for glutamate, is highly enriched at transmitter release sites (7), and is thought to act as a low pass filter at the axon terminal by inhibiting synaptic transmission upon high frequency stimulation. Mice lacking mGluR 7 exhibit increased seizure susceptibility (8), suggesting that this receptor may play a role in epileptogenesis (9). Furthermore, recent genetic association studies implicate mGluR 7 in psychiatric disorders, such as bipolar depression (10).

Different lines of evidence indicate that signal transduction by group III mGluRs is highly regulated intracellularly (5, 11). First, mGluRs 7 and 8 exist in different splice variants A and B that differ in the C-terminal sequences of their cytoplasmic tail regions. Second, the C-tails of group III mGluRs have been found to interact with various cytoskeleton-associated and Ca^{2+}-regulated proteins (5, 11). In particular, all group III mGluRs except mGluR 6 display Ca^{2+}-dependent calmodulin (CaM) binding to a conserved binding motif located in the N-terminal regions of their C-tails (12). A cluster of positively charged amino acids and a conserved serine residue (Ser^{862}) precede a hydrophobic motif containing the actual CaM-binding sequence. Based on binding experiments and sequence

* This work was supported by the Max Planck Society (to H. B.), European Community Grant QLG3-CT-2001-00929 (to H. B. and V. O'C.), Fonds der Chemischen Industrie (to H. B.), and the Wessex Medical Trust (to V. O'C.). The costs of publication of this article were defrayed in part by the payment of page charges. This article must therefore be hereby marked "*advertisement*" in accordance with 18 U.S.C. Section 1734 solely to indicate this fact.

[S] The on-line version of this article (available at http://www.jbc.org) contains supplemental Figs. S1 and S2.

[1] Present address: Max Planck Institute of Biophysical Chemistry, 37077 Göttingen, Germany.

[2] Present address: INSERM Unité 641, Université de la Méditerranée, Institut Jean Roche, Faculté de Médicine Secteur Nord, Boulevard Pierre Dramard, 13916 Marseille Cedex 20, France.

[3] Present address: Dept. of Cellular and Developmental Biology, University of Colorado Health Sciences Center, Denver, CO 80045.

[4] Present address: Dept. of Chemistry, University of Bristol, Cantocks Close, BS8 1TS Bristol, UK.

[5] To whom correspondence may be addressed: Dept. of Neurochemistry, MPI for Brain Research, Deutschordenstrasse 46, 60528 Frankfurt, Germany. Tel.: 49-69-96769-220; Fax: 49-69-96769-441; E-mail: neurochemie@mpih-frankfurt.mpg.de.

[6] To whom correspondence may be addressed: School of Biological Sciences, University of Southampton, Bassett Crescent East, Southampton S016 7PX, UK. Tel.: 44-2380592484; Fax: 44-2380594459; E-mail: jmwe@soton.ac.uk.

[7] The abbreviations used are: mGluR, metabotropic glutamate receptor; CaM, calmodulin; EF-hand, Ca^{2+}-coordinating domain with E- and F-helix; G$\beta\gamma$, G-protein $\beta\gamma$ subunits; GFP, green fluorescent protein; HEK, human embryonic kidney; ITC, isothermal titration calorimetry; mGluR 7A-C, C terminus of mGluR 7A; PDB, Protein Data Bank; PK, protein kinase; RDCs residual dipolar couplings; smMLCK, smooth muscle myosin light chain kinase; GST, glutathione *S*-transferase; BisTris, 2-[bis(2-hydroxyethyl)amino]-2-(hydroxymethyl)propane-1,3-diol.

alignment, we tentatively proposed a 1–5-10 CaM-binding motif for the C terminus of mGluR 7 (13, 14). Mutational analysis of the CaM-binding motif revealed that it overlaps with the interaction site for G-protein $\beta\gamma$-subunits ($G\beta\gamma$) (12), suggesting that Ca^{2+}/CaM may regulate signal transduction of the receptor. Consistent with this view, we found that CaM antagonists abrogate glutamatergic autoinhibition in autaptic hippocampal neurons and prevent the mGluR 7A-triggered activation of inwardly rectifying potassium channels co-expressed in HEK 293 cells (15). However, Sorensen *et al.* (16) reported that Ca^{2+}/CaM is not required for $G\beta\gamma$-mediated G-protein-coupled inwardly rectifying potassium channel activation, as signaling appeared unaffected with mutant receptors that failed to bind Ca^{2+}/CaM *in vitro*. Thus, the physiological role of Ca^{2+}/CaM binding to mGluR 7A is presently controversial. However, the stringent conservation of the CaM-binding motif in group III mGluRs strongly argues for an important function of this interaction.

CaM includes large N- and C-terminal globular domains, each including a pair of Ca^{2+}-binding EF hand motifs, EFs 1 and 2 in the N terminus and EFs 3 and 4 in the C terminus (17). Ca^{2+} ions bind to CaM in a highly cooperative manner, first to EFs 4 and 3 and subsequently to EFs 2 and 1. Ca^{2+} binding to CaM induces conformational rearrangements resulting in exposure of a hydrophobic pocket in each domain. Both pockets are capable of accommodating a large hydrophobic amino acid such as tryptophan, phenylalanine, and leucine. Target peptides adopt α-helical structures or, less commonly, β-hairpin-like loops to achieve an arrangement of key hydrophobic residues that allows binding within the two CaM pockets. As a result, the two domains of CaM effectively wrap around the target peptide; this is facilitated by a highly flexible inter-domain linker that connects the globular Ca^{2+} binding domains. Substitutions of the Ca^{2+}-coordinating residues reduce the Ca^{2+} binding affinity of the EF hands by 10–1000-fold and abolish the characteristic Ca^{2+}-induced conformational change of CaM domains (18).

Recent reports (19–21) have identified novel patterns of CaM binding to target sequences that unraveled functional differences between the two CaM lobes. Thus, CaM actions may extend over a wide spectrum, from classical binding with or without pre-association to cross-linking of two different target molecules (22). To further clarify the mode of CaM binding to group III mGluRs that are known to function as homodimers (23), we performed a detailed mutational and NMR analysis of the mGluR 7A C-tail-Ca^{2+}/CaM interaction. The results presented here show that mGluR 7A and Ca^{2+}/CaM form a classical wraparound CaM·receptor complex with a 1:1 stoichiometry and a basic 1-8-14 receptor-binding motif similar to that found in smooth muscle myosin light chain kinase. In addition, our structural data indicate that Ca^{2+}/CaM binding to mGluR 7A includes interactions with both Ser^{862}, a target site for phosphorylation by protein kinase C (13, 24, 25), and the $G\beta\gamma$ recognition motif, and thus support the view that CaM regulates signal transduction in an activity-dependent manner by competition for receptor-binding sites (15).

EXPERIMENTAL PROCEDURES

Expression Constructs—Glutathione *S*-transferase (GST) fusions of the C-terminal tail region of mGluR 7A (GST-7A-C) and of different tail mutants have been described previously (12) (see also Fig. 2). GFP fusion constructs of mGluR 7A-C were generated by subcloning the C-terminal domain into pEGFP-C2 (Clontech). *Rattus norvegicus* CaM wild type and mutant cDNA inserts were generated by PCR from rat brain cDNA or CaM cDNA, kindly donated by J. P. Adelman (26), and inserted into the pEGFP-C3 vector (Clontech) using SacI and KpnI sites. The cDNA encompassing the complete coding sequence of the rat calmodulin 1 gene was amplified from rat brain cDNA. Oligonucleotides corresponding to the 5′ and 3′ ends of the calmodulin cDNA with flanking BamHI and SalI restriction sites, respectively, were as follows: 5′-AGGGATCCTGAATGGCTGACCAACTGACTG-3′ and 5′-GTGTGGACTCACTTCGCTGTCATCATTTG-3′. Expand high fidelity (Roche Applied Science) was used in accordance with manufacturer's instruction using 2 min at 72 °C followed by 30 amplification cycles (30 s, 94 °C; 30 s, 56 °C; 30 s, 72 °C) and a final extension period of 10 min (72 °C). The flanking BamHI and SalI sites were used to clone the resulting cDNA into the pQE3 vector (Qiagen), and the resulting CAM1pQE3 plasmid was amplified in XL-1 blue cells (Stratagene, La Jolla, CA). After confirmatory DNA sequencing of the CAM1 insert in both directions, the resulting CAM1pQE3 plasmid was used for expression of untagged calmodulin; translation was driven from the authentic ATG that had been engineered directly adjacent to an artificial 5′ stop codon (TGA).

Protein Expression and Binding Studies—Expression of GST fusion proteins was performed in *Escherichia coli* BL21 DE3 (Stratagene) as described (12). HEK 293 T cells expressing GFP or GFP-7A-C (for gel filtration) and wild type or mutant GFP-CaM (for pulldown assays) were first lysed mechanically in a glass douncer in 25 mM Tris-Cl, pH 7.4, containing 100 mM NaCl, and then agitated for 1 h at 4 °C with 1.5% (w/v) Triton X-100. For pulldown assays, the detergent extracts were centrifuged at 45,000 × *g* and 4 °C for 45 min. Then 500 μl of the supernatant were incubated with 30 μl of glutathione-Sepharose beads (GE Healthcare) pre-loaded with GST-7A-C in 25 mM Tris-Cl, pH 7.4, containing 100 mM NaCl and 300 μM $CaCl_2$ or 5 mM EGTA, respectively. After 2 h of rotary agitation, beads were collected by centrifugation and washed three times with binding buffer containing $CaCl_2$ or EGTA as above. After elution with SDS sample buffer, the eluate fractions were resolved on a 10% SDS-polyacrylamide gel, followed by Western blotting with polyclonal rabbit anti-GFP (Clontech).

Determination of Molecular Size Using Gel Filtration—Supernatants of HEK detergent extracts were directly used for gel filtration experiments. Proteins were separated on a pre-packed Superose 12 PC 3.2/30 column using a Smart system (GE Healthcare). The running buffer was 25 mM Tris-Cl, 100 mM NaCl, pH 7.4; 300 μM $CaCl_2$ or 5 mM EGTA was added as indicated. The column was calibrated by using blue dextran for exclusion volume determination or 50 μl of a mixture of proteins of known size (chymotrypsinogen, ovalbumin, and albumin; Bio-Rad). Protein elution was monitored by absorption at

280 nm or Western blot analysis of eluate fractions. GFP or GFP-tagged proteins were visualized at their absorption maximum (488 nm) using a μPeak monitor with a wavelength accuracy of 2 nm and a spectral bandwidth of 4 nm. Elution curves were evaluated using the Smart Manager software (GE Healthcare).

Isothermal Titration Calorimetry—Isothermal titration calorimetry (ITC) was performed at 32 °C on a Microcal VP-ITC calorimeter (Microcal, Northampton, MA). CaM and peptide were prepared and dialyzed in the same buffer (20 mM BisTris, 300 mM KCl, 6 mM $CaCl_2$, pH 6.8). All samples were degassed before use. In the syringe, the peptide concentration was 500 μM, whereas the CaM concentration in the sample cell was 20 μM. ITC measurements were performed with 18 injections of 6 μl of peptide solution into the cell containing CaM while stirring at 310 rpm. Heats of dilution were corrected using the last titration points, and data were analyzed using the Wiseman isotherm for a one-site binding model as implemented in the Microcal Origin software.

NMR Sample Preparation—For protein expression, the CAM1pQE3 vector was transformed into *E. coli* BL21 DE3 (Stratagene) and initially screened for protein expression using isopropyl 1-thio-β-D-galactopyranoside induction (1 mM) in 1-ml mini-cultures (Qiagen). Uniformly labeled recombinant CaM was overexpressed in *E. coli* (BL21 DE3) grown solely on M9 media supplemented with 1 g/liter $^{15}NH_4Cl$ and 2 g/liter $^{13}C_6$-D-glucose. Prior to induction, the cultures were incubated at 37 °C before being cooled to 30 °C and subsequent incubation with isopropyl 1-thio-β-D-galactopyranoside for 18 h. Cells were harvested after 18 h, and labeled CaM was purified to homogeneity (27) using phenyl-Sepharose chromatography. Peptides corresponding to the mGluR 7 CaM binding region were synthesized using standard solid phase technology (Peptide Protein Research, Fareham, UK). NMR samples were prepared as 1 mM CaM in 20 mM BisTris, 300 mM KCl, 6 mM $CaCl_2$, pH 6.8, 0.05% NaN_3 in 600 μl of 5% D_2O in H_2O for assignment purposes. Such samples were diluted with the aforementioned buffer to half the original CaM concentration for relaxation and residual dipolar coupling (RDC) measurements. The molar ratio of peptide to CaM used was 1.1:1. Aligned samples were prepared by adding a pre-dried 600-μl volume, 5 mm diameter, 5% polyacrylamide gel to a 600-μl 0.5 mM CaM sample and allowing the gel to swell for 48 h at 4 °C prior to insertion into a 5-mm NMR tube and data collection. Peptides corresponding to the mGluR 7A, residues 856–875, 856–875 phosphorylated at Ser-862 and Ser-856–879, mGluR 7A-(856–875), Ser(P)^{862}-mGluR 7A-(856–875), and mGluR 7A-(856–879), respectively, were purchased from Protein Peptide Synthesis (Peptide Protein Research, Fareham, UK).

NMR Measurements—All NMR experiments were recorded on a Varian Inova 600-MHz spectrometer at 32 °C. Backbone assignments of Ca^{2+}/CaM and the peptide complexes thereof were achieved using three-dimensional HNCACB (28, 29) and CBCACONH (30) experiments. Chemical shift perturbations (Δ) of the [^{1}H]-^{15}N spectra with and without ligand were calculated using combined ^{1}H and ^{15}N chemical shifts (δ) as shown in Equation 1,

$$\Delta\delta = \sqrt{\Delta\delta(^1H)^2 + \frac{1}{36}\Delta\delta(^{15}N)^2} \quad \text{(Eq. 1)}$$

The dissociation constant of the Ser(P)^{862}-mGluR 7A-(856–875)·Ca^{2+}/CaM complex was determined by chemical shift titration. Two 0.1 mM samples of CaM were prepared in 20 mM BisTris, 300 mM KCl, 6 mM $CaCl_2$, 0.05% NaN_3, pH 6.8. One sample was supplemented with Ser(P)^{862}-mGluR 7A-(856–875) to 2 mM (20:1 ratio), and the pH adjusted to 6.8. [^{1}H]-^{15}N HSQC spectra were recorded on each of these samples before aliquots of peptide sample were added to the CaM only sample to achieve peptide to protein ratios of 0:0, 0.5:1, 1:1, 2:1, 4:1, 8:1, and 12:1. The combined ^{1}H and ^{15}N chemical shifts of residues in fast exchange were analyzed using $y = [X]/(K_D + [X])$, where y is the fractional shift; $[X]$ is the peptide concentration, and K_D is the dissociation constant.

The dependence of RDCs on the relative orientations of the amide bonds provides powerful constraints on the solutions structure of molecules. Here, RDCs were used to investigate the solution structures of the CaM domains in the complexes and their relative orientation (31). Provided a structure of a domain is known, the RDCs define an alignment tensor that is characterized by axial and rhombic components A_a and A_r, respectively, indicating the strength of the alignment of a domain as well as three rotation angles (Euler angles α, β, and γ) that give the orientation of the tensor with respect to the molecular frame of the domain. By comparing alignment tensors of one domain to the other one can define the overall structure of the domains and in favorable cases get an indication of interdomain dynamics. In a compact well structured state the two domains of CaM are described by a common molecular frame, and consequently the axial and rhombic components A_a and A_r of the domains are expected to be within experimental error. By the same token, the interdomain orientation in solution of the complex in question is determined by rotating the molecular frames of the N- and C-terminal domains such that the alignment tensors of the individual domains are colinear. NMR data recorded on aligned samples revealed negligible chemical shift changes when compared with the isotropic data indicating the effects of the gel matrix on the protein structure to be minimal. [^{1}H]-^{15}N dipolar couplings were recorded using 0.5 mM Ca^{2+}/CaM, mGluR 7A-(856–875):Ca^{2+}/CaM, and mGluR 7A-(856–879):Ca^{2+}/CaM samples with a 1.1:1 stoichiometry and were measured from two-dimensional IPAP-type sensitivity-enhanced experiments (32), which had been recorded with an acquisition time of 152 ms in the nitrogen dimension. Errors in the RDCs were estimated to be 0.5 Hz. In the mGluR 7A-(856–875)·Ca^{2+}/CaM complex, 31 and 37 RDCs were determined, whereas in the mGluR 7A-(856–879)·Ca^{2+}/CaM complex, 57 and 52 RDCs were resolved in the N- and C-terminal calmodulin domains, respectively. The agreement between the data and the structures was evaluated using a quality factor Q as shown in Equation 2 (33).

$$Q = \sqrt{\sum(rdc^{\text{measured}} - rdc^{\text{calculated}})^2} \Big/ \sqrt{\sum(rdc^{\text{measured}})^2} \quad \text{(Eq. 2)}$$

Comparisons of the RDC data were restricted to x-ray struc-

tures of moderate to good resolution in the Protein Data Base. ^{15}N relaxation time constants were calculated from a series of seven two-dimensional ^{15}N T_1 and T_2 relaxation spectra (34, 35) recorded with relaxation delays of 0.02, 0.08, 0.16, 0.32, 0.6, 1, and 1.5 s and 0.01, 0.03, 0.05, 0.07, 0.09, 0.13, and 0.15 s for T_1 and T_2, respectively. Data were processed with mild resolution enhancement and zero filling in the proton dimension and linear prediction in nitrogen. All data were processed using NMRPipe and NMRDraw (36) and analyzed using NMRview (37). Rotational correlation times were calculated from the average T_1:T_2 ratio of residues in secondary structural elements only.

Molecular Modeling and Structure Refinement—Mutations introduced into the *R. norvegicus* CaM and peptide sequences were modeled using Pymol (DeLano Scientific, San Carlos, CA) based on the backbone coordinates of the high resolution structure of CaM complexed with the CaM binding region from smooth muscle myosin light chain kinase (smMLCK, PDB entry 1qtx). Alignment tensors were calculated for each CaM domain (N-domain including residues 1–75 and C-domain including residues 76–148) from [^{1}H]-^{15}N RDC data in secondary structural elements using the program Module (38). For the calculation, 57 and 52 RDCs were used in the N- and C-terminal domains, respectively. The resulting alignment tensors of the N- and C-terminal domains were rotated into a common coordinate frame by rigid body rotation of the C-terminal domain. The relative orientation of the domains was then fixed, and the C-domain was translated to optimize the inter-domain docking of helices 2 and 6 observed in the smMLCK·CaM complex. The inter-domain linker was allowed to break between residues 75 and 76 to achieve this. The resulting structure was annealed using the constant valence force field CVFF (39) in the Discover module of InsightII (Accelrys Software Inc). Backbone atoms of residues 1–73 and 78–148 and all atoms of Ca^{2+}-coordinating residues were fixed during the annealing protocol. CaM mGluR 7A interactions were defined using a upper distance criterion of 4 Å.

RESULTS

Mutation of the Ca^{2+}-binding Sites in the C-terminal Lobe of CaM Impairs mGluR 7A-C Binding—To analyze the contributions of the N- and C-terminal lobes of CaM to mGluR 7A binding, we generated GFP-tagged constructs encoding CaM carrying previously characterized point mutations of the Ca^{2+} coordinating residues in its four EF-hands (26, 40). The ability of the mutant and wild type CaM to bind GST-7A-C was then examined by using a pulldown assay. Aspartate was mutated to alanine either in the N-terminal (CaM 1,2), C-terminal (CaM 3,4) or both EF-hand pairs (CaM 1–4), the latter resulting in a Ca^{2+}-insensitive CaM (20, 41) (Fig. 1). Wild type CaM and CaM 1,2 were found to effectively bind GST-7A-C in a Ca^{2+}-dependent manner, whereas CaM 1–4 did not detectably interact. Compared with wild type CaM, binding of GFP-CaM 3,4 was significantly reduced. Thus, the two lobes of CaM contribute differently to Ca^{2+}-dependent mGluR 7A-C binding.

Binding of Endogenous Ca^{2+}/CaM Causes a Size Shift of GFP-7A-C—Metabotropic glutamate receptors are known to function as dimers (23), although previous fluorimetric studies with dansylated CaM have indicated a 1:1 stoichiometry of the

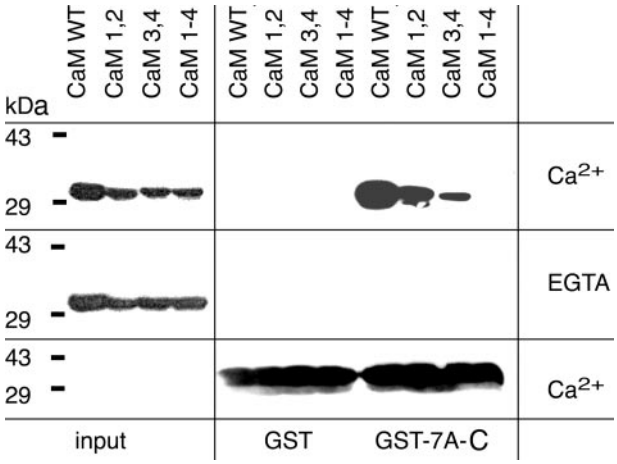

FIGURE 1. **Ca^{2+}-binding sites in the C-terminal lobe of CaM are essential for binding to mGluR 7A-C.** Pulldown assays using immobilized GST, or GST-7A-C, are shown. HEK 293 T cell lysates were tested for expression of GFP-CaM wild type and mutants (*left*) and incubated with the GST fusion proteins in the presence of 300 μM Ca^{2+} or 5 mM EGTA, respectively (*right*). After washing, bound proteins were eluted with SDS sample buffer and analyzed by 10% SDS-PAGE and Western blotting with antibody directed against GFP (*top panels*) or GST (*bottom panel*; loading control). Note that only CaM wild type and CaM 1,2, but not CaM 3,4 and CaM 1–4, bound efficiently to GST-7A-C.

mGluR 7A-C-Ca^{2+}/CaM interaction (12). As the data presented above revealed only a minor contribution of the N-lobe of CaM to mGluR 7A binding, we wondered whether this region of CaM could serve as a binding site for a second target molecule, resulting in 1:2 CaM:target or 2:2 CaM:target stoichiometries, as described for other CaM interactors (reviewed in Ref. 22). We therefore performed gel filtration experiments on a calibrated Sepharose PC12 column. In initial experiments, we determined the size of complexes formed by recombinant GST-7A-C and purified bovine brain CaM. An interaction was detectable in the presence of 300 μM Ca^{2+}, but the stoichiometry could not be reliably evaluated, as both interaction partners ran as homodimers (data not shown). To overcome this limitation, we employed GFP-7A-C fusion proteins expressed in mammalian cells, which could be readily detected in cell lysates at the maximum excitation wavelength of GFP (488 nm) (Fig. 2). In addition, absorbance measurements at 488 nm were confirmed by Western blotting with an anti-GFP antibody (data not shown).

The elution patterns of GFP-7A-C and the truncated version GFP-7A-N38 (Fig. 2*E*) are presented in Fig. 2. Both proteins contain the Ca^{2+}/CaM binding domain (12) and were tested for differences in elution positions in the presence of either 300 μM Ca^{2+} or 5 mM EGTA. Both GFP-7A-C (Fig. 2*A*) and GFP-7A-N38 (Fig. 2*B*) ran as narrow peaks in the presence of EGTA and as wider asymmetrical peaks in the presence of Ca^{2+}, respectively. Notably, the EGTA peaks in Fig. 2*B* were eluted at a later volume as compared with Fig. 2*A*, consistent with the deletion of 27 amino acids in the GFP-7A-N38 protein. In 300 μM Ca^{2+}, a size shift toward a lower elution volume was observed with both proteins. This size shift was because of an interaction with endogenous Ca^{2+}/CaM, because GFP-7A F863A, a mutant that does not bind Ca^{2+}/CaM (12), eluted at identical positions under both conditions (Fig. 2*C*). The only partial size shifts seen in Fig. 2, *A* and *B*, in the presence of Ca^{2+} presumably reflect

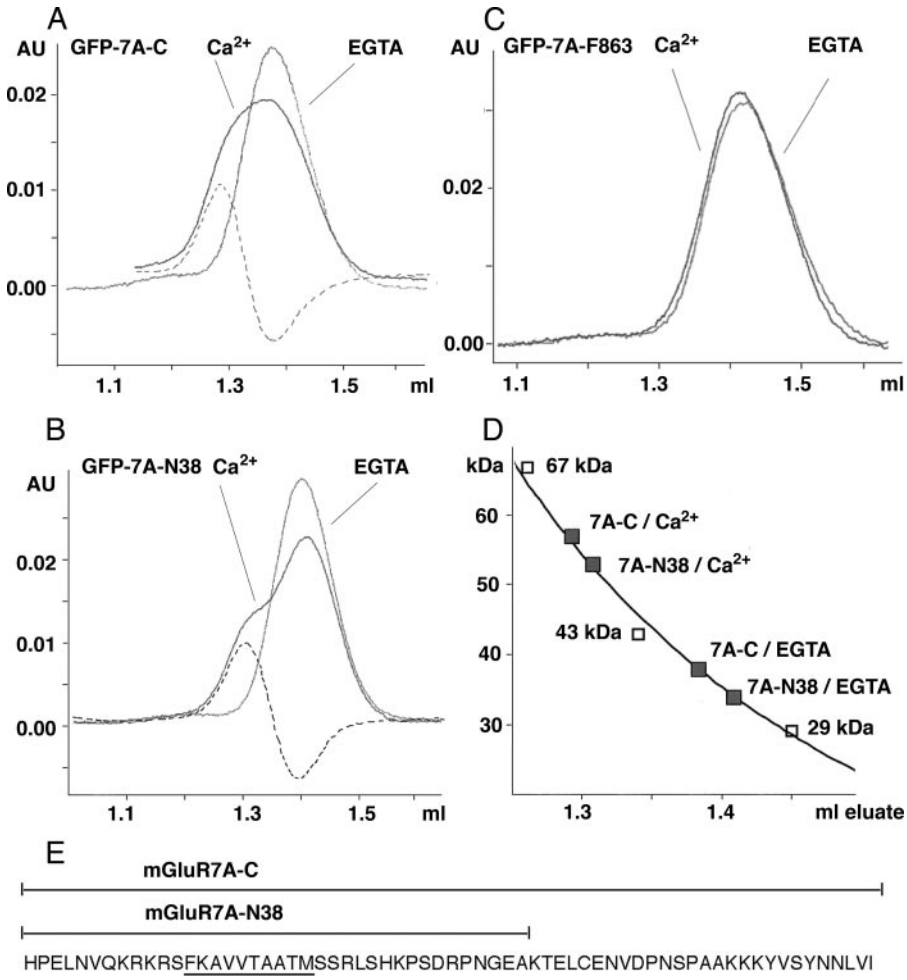

FIGURE 2. **Analysis by gel filtration of Ca^{2+}/CaM binding to mGluR 7A-C.** GFP-7A-C shows a size shift in the presence of Ca^{2+}. Overlay of elution curves of GFP-7A-C (*A*) or GFP-7A-N38 (*B*) obtained in 5 mM EGTA and 300 μM Ca^{2+}, respectively, is displayed as detected at 488 nm. Note that the elution profiles obtained in Ca^{2+} show shoulders. Subtraction of both curves (*dotted lines* in *A* and *B*) illustrates the fraction of GFP fusion protein that underwent a size shift toward a higher molecular weight. *C* shows that GFP-7A F863A, a mutant known not to bind Ca^{2+}/CaM, does not undergo a size shift in the presence of Ca^{2+}. *D* shows a plot of the elution peak volumes determined in A-C at 488 nm (in ml; *filled squares*) together with the elution volumes of proteins of known molecular weight (monitored at 280 nm; *open squares*). *E*, sequence of mGluR 7A-C (residues 851–915). The mGluR-N38 truncation used in *B* is indicated *above* the sequence. The CaM binding region is *underlined*.

saturation of the endogenous CaM by other interacting proteins.

To quantify the size shifts depicted in Fig. 2, *A* and *B*, we subtracted the elution profiles obtained in the presence of EGTA from those in Ca^{2+}-containing buffer, yielding peaks that represent only the fractions of the GFP fusion proteins that altered positions (Fig. 2, *A* and *B*, *dotted lines*). When plotting the respective elution positions against those of marker proteins of known molecular weight, differences of about 19 and 20 kDa were found for GFP-7A-C and GFP-7A-N38 (Fig. 2*D*), respectively. This value corresponds to the approximate predicted molecular size of CaM and confirms a 1:1 stoichiometry of mGluR 7A-C binding to native Ca^{2+}/CaM.

Structural Analysis of the mGluR 7A-C CaM Interaction—The binding region of mGluR 7A (comprising residues 860–876) contains two pairs of hydrophobic residues with correct spacing to bind CaM, suggesting that two different modes of CaM binding could exist. The interaction of Ca^{2+}/CaM with mGluR 7A-C was therefore investigated further using NMR spectroscopy. To this end, two peptides were synthesized comprising the CaM binding region. They correspond to residues 856–875 and 856–879 of mGluR 7A (Fig. 3*A*). The shorter mGluR 7A-(856–875) peptide is representative of a basic-1–10 motif similar to that found in CaM kinase IIα (42) and predicted to utilize Phe^{863} and Met^{872} as binding residues for the exposed hydrophobic sites of Ca^{2+}/CaM. The extended mGluR 7A-(856–879) sequence represents a basic 1-8-14 motif similar to that found in smooth muscle myosin light chain kinase (43) and as such should dock to Ca^{2+}/CaM using Phe^{863} and Leu^{876}. The mGluR 7A sequence is unusual in that instead of a basic residue a serine (Ser^{862}) precedes the phenylalanine, which is the site of phosphorylation by protein kinase C (13, 24). Phosphorylation at equivalent sites in other binding sequences has been shown to greatly reduce the affinity for Ca^{2+}/CaM. The dissociation constant of mGluR 7A-(856–875)·Ca^{2+}/CaM complex was determined by ITC to be 100 nM with a 1:1 stoichiometry (supplemental Fig. S1). This dissociation constant dropped by about 1000-fold when the mGluR 7A-(856–875) peptide was phosphorylated at Ser^{862} (supplemental Fig. S2).

Incubation of both mGluR 7A-(856–875) and mGluR 7A-(856–879) with Ca^{2+}/CaM at peptide to protein ratios of 1.1:1 completely converted free CaM to the complexed form, as observed by their ^{1}H amide and ^{15}N chemical shifts. Changes in amide chemical shift upon complex formation with mGluR 7A-(856–875) and mGluR 7A-(856–879) are shown in Fig. 3, *B* and *C*, respectively. The data clearly show that both peptides affect the structure of the N- and C-lobes of CaM. A number of signals from residues in the central linker of CaM in the mGluR 7A-(856–875)·Ca^{2+}/CaM complex were too broad to be observed in NMR spectra. The reappearance of these peaks in the mGluR 7A-(856–879)·Ca^{2+}/CaM spectra together with modest chemical shift changes as compared with the free state suggests that the linker is stabilized upon binding of the extended peptide. The modest chemical shift differences between the mGluR 7A-(856–875) and mGluR 7A-(856–879) complexes (Fig. 3*D*) indicate similarity between the structures of the two peptide protein complexes. Moreover, they provide insight into the orientation of the peptide with respect to the two CaM domains. The largest chemical shift differ-

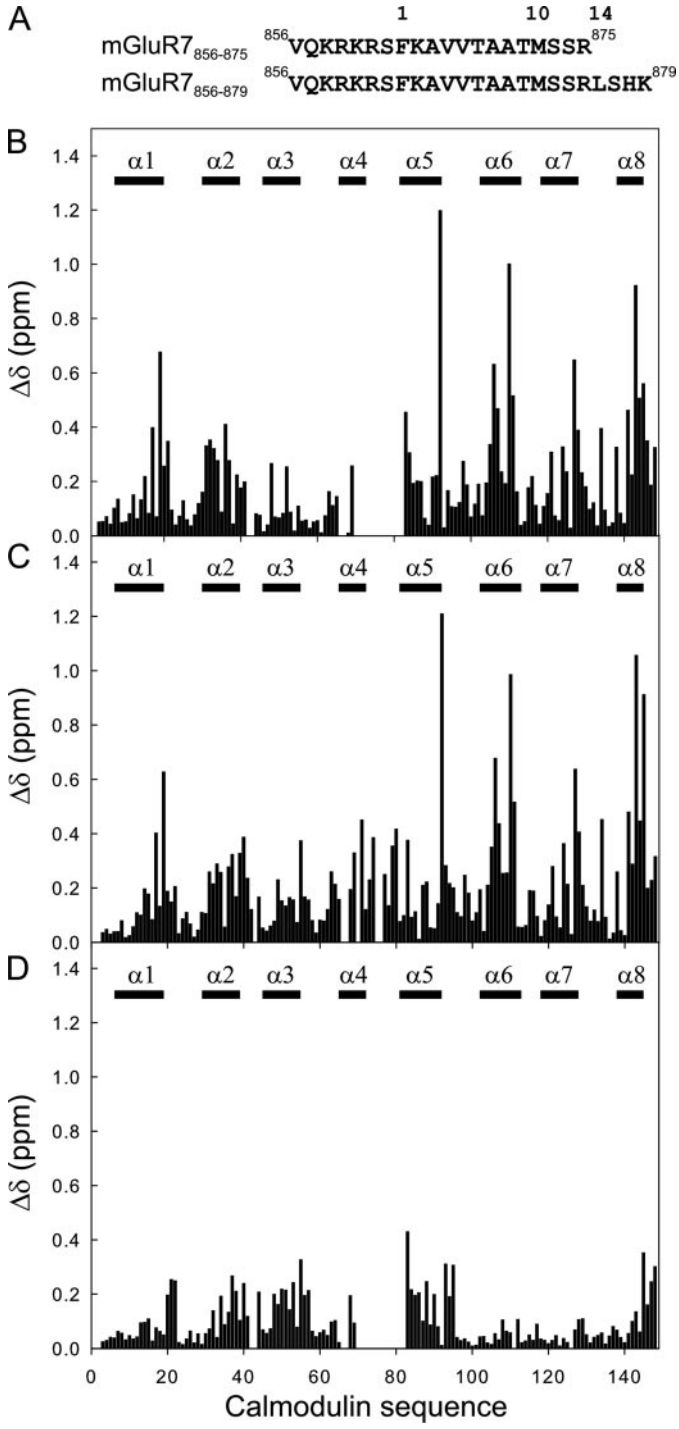

FIGURE 3. **Interaction of CaM with the mGluR 7A binding region.** Amino acid sequence of the peptides mGluR 7A-(856–875) and mGluR 7A-(856–879) is shown; *numbers* above the sequence indicate position of hydrophobic anchor residues (*A*). Chemical shift perturbation of CaM backbone amide groups is shown in the presence of mGluR 7A-(856–875) (*B*) and mGluR 7A-(856–879) (*C*). Chemical shift differences between the Ca^{2+}/CaM·mGluR 7A-(856–875) and Ca^{2+}/CaM·mGluR 7A-(856–879) complexes are shown in *D*. $\Delta\delta$ is the chemical shift difference of the combined ^{1}H and ^{15}N shifts. The positions of CaM helices are indicated by *black bars* and numbered from the N to the C terminus.

ences between the two peptide·Ca^{2+}/CaM complexes are seen in the C-lobe. These only occur in helix 5, which is adjacent to the interdomain linker and the C terminus, whereas otherwise the chemical shift differences in the two complexes in this lobe are very small. In contrast, the N-lobe is more globally altered upon extension of the peptide with the exclusion of helix 1 (Fig. 3*D*). This suggests that the C-terminal extension of mGluR 7A-(856–879) is located near helix 5 and the interdomain linker of CaM. In this orientation the observations of differences in helix 2 and 3 of the N-terminal CaM lobe for the extended peptide are consistent with a wraparound CaM structure (see below).

Rotational correlation times (τ_c) of CaM were determined using ^{15}N relaxation measurements and used to characterize interdomain dynamics. The N- and C-lobes had correlation times of 7.1 ± 0.1 and 6.5 ± 0.1 ns, respectively, which is in good agreement with the literature values of 7.1 and 6.3 ns of similar calmodulin peptide complexes (44). Dynamics analysis of the truncated determinant mGluR 7A-(856–875)·Ca^{2+}/CaM complex revealed a narrowing in the range of T_1s and T_2s, consistent with a reduction in the plasticity of the CaM domains. The correlation times for mGluR 7A-(856–875)·Ca^{2+}/CaM N- and C-lobes were determined to be 7.1 ± 0.1 and 7.2 ± 0.1 ns, respectively, indicating that the two domains now tumble at similar rates. This information, coupled with the 1:1 peptide:CaM stoichiometry, indicates that the mGluR 7A-(856–875)·Ca^{2+}/CaM complex adopts the classical wraparound structure common to most CaM·peptide complexes (43, 45, 46). Similarly, τ_c values calculated for the N- and C-lobes in the mGluR 7A-(856–879)·Ca^{2+}/CaM complex were 7.9 ± 0.1 and 7.8 ± 0.1 ns, respectively. These values are in good agreement with the correlation time of 7.6 ns that was recorded for comparable peptide complexes, such as the 26-mer olfactory CNG channel fragment·CaM complex (47) when considering that those data were collected at 35 °C rather than at 32 °C as used here.

Further insight into the nature of the interaction between the CaM and the mGluR 7A-C peptides was obtained by measuring ^{1}H-^{15}N RDCs for both the mGluR 7A-(856–875)·Ca^{2+}/CaM and mGluR 7A-(856–879)·Ca^{2+}/CaM complexes (Fig. 4). It can be seen in Fig. 4, *A* and *B*, that good correlations of measured and calculated RDCs were found for both complexes when the RDCs were calculated using the CaM domain from smMLCK (PDB entry 1qtx) in complex with the RS20 peptide. Differences in the strength of the alignment of individual domains as reflected by differences in the values for the axial and rhombic components of the alignment tensors A_a and A_r of the individual domains are qualitative indicators of interdomain motion. The largest difference in alignment of the N- and C-lobes was found for the rhombic component of free CaM (data not shown); this is consistent with the presence of interlobe motion. In contrast, the differences in alignment and domain orientation between the N- and C-lobes in the mGluR 7A-(856–879)·Ca^{2+}/CaM complex are very small (Fig. 4*D*). This is indicative of a compact globular structure. Overall the alignment tensors of the lobes in the mGluR 7A-(856–875)·Ca^{2+}/CaM complex are similar but not quite as co-linear as in the complex with the extended mGluR 7A sequence (Fig. 4*C*). Using the smMLCK:CaM coordinates as a model for the mGluR 7A-(856–879)·Ca^{2+}/CaM complex, helices 2 and 3 in the N-lobe and helix 5 of the C-lobe of CaM are surrounding the extra four residues of mGluR 7A-(856–879). This is consistent

with the chemical shift changes observed between the binding of mGluR 7A-(856–875) and mGluR 7A-(856–879) (Fig. 3*D*), as well as with the observed changes in the line shapes of the preceding interdomain linker. The combined RDC and chemical shift data provide good evidence for a classic wraparound structure of the Ca^{2+}/CaM·mGluR 7A complex.

Residual dipolar couplings have been used successfully to classify CaM-binding motifs present in the protein kinase family (48) and, more recently, to evaluate motifs outside the kinase family (47). The latter proved to be successful only if the RDCs used in the analysis were restricted to those residues located in structured regions of CaM. The binding modes of the mGluR 7A peptides were tested by fitting the RDCs of the mGluR 7A-(856–875)·Ca^{2+}/CaM and mGluR 7A-(856–879)·Ca^{2+}/CaM complexes to the coordinates of 13 CaM·peptide complexes, including examples from the 1-8-14, 1-10, 1-16, and IQ motifs and the peptide-free closed form of CaM (PDB entry 1prw) as well as more unusual binding modes, such as that of the glutamate decarboxylase·CaM complex (PDB entry 1nwd) where two helical peptides were observed to bind between the CaM domains. As a result for each structure, one obtains two alignment tensors (one for each domain) together with measures of the quality of the fit. The results of fitting 13 structures to the RDC data were evaluated using the quality of the agreement between the structure and the data as quantified by the quality factor *Q*, and the agreement between the domain orientations of the tested structures with the data as shown by small domain rotations ($\Delta\alpha$, $\Delta\beta$, and $\Delta\gamma$) required to obtain co-linearity of the alignment tensors of the CaM domains. The same analysis was applied to RDCs of the shorter mGluR 7A-(856–875)·Ca^{2+}/CaM (data not shown) and extended mGluR 7A-(856–879)·Ca^{2+}/CaM complexes (Table 1).

The best (lowest) *Q* value and the best fit of the alignment tensors for both the mGluR 7A-(856–875)·Ca^{2+}/CaM and mGluR 7A-(856–879)·Ca^{2+}/CaM complexes were obtained when the RDC data were compared with the crystal structure of smMLCK. This was surprising

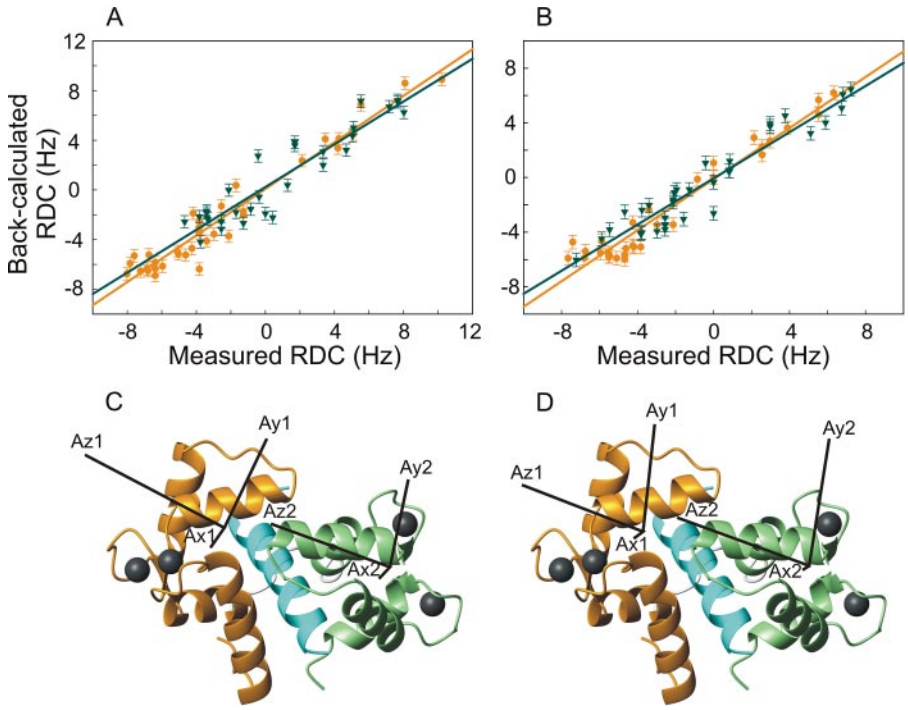

FIGURE 4. **Domain orientation of CaM/mGluR 7A binding region complexes.** Correlation and linear regression between measured dipolar couplings of mGluR 7A-(856–875)·Ca^{2+}/CaM (*A*) and mGluR 7A-(856–879)·Ca^{2+}/CaM (*B*) are shown with back-calculated dipolar couplings using the N- and C-terminal domains of the smMLCK peptide complex (PDB entry 1qtx) individually, and ribbon diagrams of smMLCK peptide complex with alignment tensors for the N- and C-terminal domains of mGluR 7A-(856–875)·Ca^{2+}/CaM (*C*) and mGluR 7A-(856–879)·Ca^{2+}/CaM are shown in *D*. Data and ribbon representations corresponding to the N-terminal domain, C-terminal domain and the peptide are in *gold, green* and *cyan,* respectively. Bound Ca^{2+} atoms are shown as *black spheres*. The figure was created using MolMol (57).

TABLE 1
Summary of alignment tensors for the CaM·mGluR $7A_{856-879}$ complex

Structure[a]	Binding motif[b]	*Q*[c]	$\Delta\alpha$[d]	$\Delta\beta$[d]	$\Delta\gamma$[d]	ΔA_a[e]	ΔA_r[e]	$\langle\chi^2\rangle$[f]
1QTX (1.65 Å)	Basic 1-8-14	0.29	−6.7	1.7	−5.7	0.18	−0.11	298
1QS7 (1.8 Å)	Basic 1-8-14	0.33	−5.5	5.1	20.1	0.07	0.02	379
1MXE (1.7 Å)	1-14	0.33	3.4	3.0	−12.0	−0.21	0.02	387
1WRZ (2.0 Å)	Basic 1-5-8-14	0.36	−22.8	−0.8	−1.8	0.07	−0.02	427
1NIW (2.0 Å)	Basic 1-5-8-14	0.36	311.3	11.4	32.7	0.03	0.35	421
1CDL (2.0 Å)	Basic 1-8-14	0.37	−8.1	0.7	−10.7	0.41	−0.13	477
2F3Y (1.4 Å)	1-10	0.31	160.9	−39.7	151.7	−0.17	−0.25	352
1CDM (2.0 Å)	Basic 1-10	0.32	16.2	−10.9	1.9	0.18	−0.11	374
1IQ5 (1.8 Å)	1-16	0.30	22.2	−30.4	−1.4	−0.08	−0.03	320
1IWQ (2.0 Å)	1 hydrophobic	0.32	−149.6	−26.3	172.6	−0.02	0.02	358
1L7Z (2.3 Å)	NA	0.34	6.7	−17.3	16.4	−0.24	0.00	413
2F2O (2.2 Å)	NA	0.51	149.0	−7.6	−168.6	−0.14	0.11	891
1PRW (1.7 Å)	No peptide	0.35	163.0	−18.3	−181.6	0.23	−0.28	444

[a] PDB entry codes and resolution for structures that were tested are shown.
[b] Structures were classified according to their binding motifs as proposed in Ref. 50.
[c] The quality factor *Q* measures the agreement between the data and the structures.
[d] $\Delta\alpha$, $\Delta\beta$, and $\Delta\gamma$ represent the difference in α, β, and γ Euler angles, respectively, between the N- and C-domains of CaM in the mGluR $7A_{856-879}$·Ca^{2+}/CaM complex.
[e] $\Delta\alpha$ and ΔA_r denote the difference in the axially symmetric and rhombic components of the alignment tensors between N- and C-domains.
[f] $\langle\chi^2\rangle$ values are the mean of the total $\langle\chi^2\rangle$ values for the N- and C-domains of CaM in the mGluR $7A_{856-879}$·Ca^{2+}/CaM complex.

because the smMLCK structure is an example for a binding mode of a basic 1-8-14 motif, whereas the mGluR 7A-(856–875) peptide is lacking the anchor residue leucine (Leu^{876}) at position 14. This suggests that the second large hydrophobic residue is not required for either complex formation or maintenance of structural integrity. This is further supported by inspection of the *Q* values and Euler angles of the other structures that contain 1-14 or basic 1-8-14 motifs. The majority of those structures fit the data for the mGluR 7A·Ca^{2+}/CaM peptide complexes well and generally better than complexes with other motifs. In our case, however, comparison of *Q* values across structures representing different binding motifs was not sufficient to determine the binding mode, because the second and third lowest *Q* values were obtained with structures that have either 1-16 (PDB entry 1iq5) or 1-10 (PDB entry 2f3y) motifs. Interestingly, both of these structures require significant domain reorientations to agree with the solution structures, as indicated by large values for either $\Delta\alpha$, $\Delta\beta$, or $\Delta\gamma$ in Table 1. This suggests that the fold of a CaM·peptide complex may not be dictated by the spacing of the observed anchoring residues of the peptide, because our RDC data, when compared across a full range of CaM structures, did not closely match all structures of a certain motif.

Modeling of the Interaction of Ca^{2+}/CaM with mGluR 7A—To further analyze the interaction between mGluR 7A and the N- and C-lobes of CaM, we modeled the mGluR 7A-(856–879)·Ca^{2+}/CaM complex using the smMLCK CaM structure as a template. This crystal structure shows a collapsed CaM conformation bound at a 1:1 stoichiometry. Similar to the target sequence in smMLCK, the CaM binding region of mGluR 7A adopts an α-helical conformation, as evidenced from filter-edited NMR data collected on a sample of ^{13}C, ^{15}N-CaM in complex with unlabeled

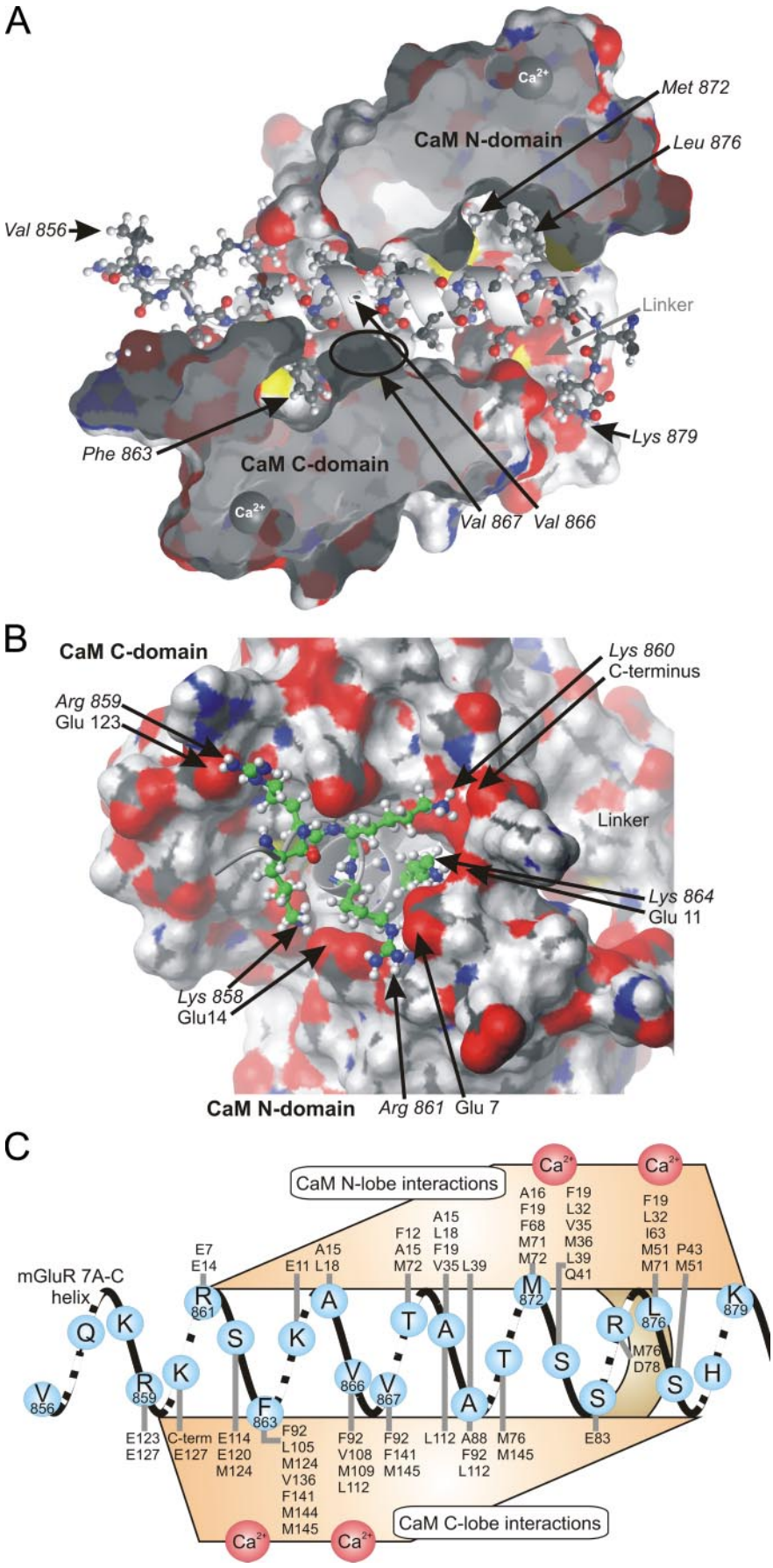

mGluR 7A-(856–875) peptide (data not shown). After rotating the N- and C-terminal domains to satisfy the RDC data and docking the mGluR 7A-(856–879) peptide in CaM according to the positioning in the rotated smMLCK complex, the structure was energy-minimized. The resulting structure showed good overall energies and no steric clashes. Fig. 5 shows a surface representation of the resulting structural model. Accordingly, anchor residues 1 (Phe^{863}) and 5 (Val^{867}) of the mGluR 7A binding domain point into the hydrophobic pocket of the C-lobe of CaM, whereas residues 10 (Met^{872}) and 14 (Leu^{876}) are located in the pocket of the N-lobe (Fig. 5, *A* and *B*).

The following side chain interactions were predicted with the C-lobe of CaM. Based on interatomic distances, the first residue (Phe^{863}) of the 1-8-14 motif (Fig. 5*C*) is likely to interact with a number of hydrophobic residues in the C-lobe of CaM that form a hydrophobic pocket (Phe^{92}, Leu^{105}, Met^{124}, Val^{136}, Phe^{141}, Met^{144}, and Met^{145}). The central anchor residue (Val^{867}) is also located within the same hydrophobic pocket (interactions to Phe^{92}, Phe^{141}, and Met^{145}). Another hydrophobic residue is the preceding residue Val^{866} (Fig. 5*C*), which may interact with the CaM residues Phe^{92}, Val^{108}, Met^{109}, and Leu^{112} and is located at position 4 of the CaM-binding motif. In addition there are electrostatic interactions. The C-terminal end of the peptide binding channel of CaM is known to have a negatively charged rim, whereas the N-lobe is thought to present clusters of negatively and positively charged residues (43, 45, 49). These surface charges contribute to peptide binding via electrostatic interactions and are thought to determine the relative orientation of the CaM binding domain peptides on the C-lobe (50). In agreement with this idea, our model suggests electrostatic interactions between Arg^{859} of mGluR 7A and CaM residues Glu^{123} and Glu^{127} and between Lys^{860} and residues Glu^{127} and the C-terminal carboxyl group of CaM (Fig. 5*C*).

The model also predicts interactions with the N-lobe of CaM: The hydrophobic residue Met^{872} of mGluR 7A points toward the hydrophobic patch of the calmodulin N-lobe and lies in close vicinity of CaM residues Phe^{19}, Phe^{68}, Met^{71}, and Met^{72} (Fig. 5*C*). An additional hydrophobic residue in position 14 (Leu^{876} of mGluR 7A) is predicted to interact with the N-lobe, whereas in the CaM structure of smMLCK the apolar residue Asn^{312} is located at this position (45). For both Asn^{312} and the following hydrophobic residue Phe^{313} of the smMLCK CaM structure, no interaction with the N-lobe has been reported. In contrast to previous studies (50), ionic interactions between mGluR 7A and the charged rim of the N-lobe were only found between negatively charged side chains of CaM and basic residues of mGluR 7A (Fig. 5*B*). Arg^{861} of mGluR 7A is predicted to interact with Glu^{7} and Glu^{14} of CaM. Ser^{862} is within hydrogen bonding space of both Glu^{14} and Glu^{120} of calmodulin. This serine is of particular interest as its phosphorylation reduces the binding constant of mGluR 7A-(856–875) to CaM by about 1000-fold and abolishes CaM binding (13) which, based on our model, would be explained by anionic repulsion.

Binding Studies with Targeted mGlu7A-C Point Mutations Corroborate the Modeling Predictions—Previous experiments had already shown that binding to wild type CaM is abolished upon mutation of the hydrophobic anchor residue 1 (F863A), whereas substitution of residue 10 by alanine (M872A) did not interfere with binding (12). Here we dissected the individual contributions of the N- and C-lobes to mGluR 7A binding by mutating hydrophobic (Phe^{863}, Val^{867}, Val^{868}, Met^{872}, and Leu^{876}) and charged (Arg^{859}, Arg^{861}) residues in GST-7A-C. The binding properties of the resulting fusion proteins were tested in pulldown assays with a panel of GFP-tagged CaM constructs consisting of the wild type protein and the EF hand mutants CaM 1,2, CaM 3,4, and CaM 1–4. Fig. 6 shows that substitutions of all residues in GST-7A-C that interact with the C-lobe impede binding to CaM proteins (Fig. 6, *top half*), whereas mutations of residues interacting with the N-terminal domain retained residual binding except in case of CaM 1–4 (Fig. 6, *bottom half*). This corroborates the notion that the interaction of GST-7A-C with the C-lobe provides most of the binding energy.

The most profound reduction in CaM binding was seen upon alanine substitution of the anchor residue Phe^{863} (position 1 in the 1-8-14 motif of mGlu7A-C) which interacts with the C-lobe. This mutation abrogated binding to both wild type and mutant CaMs. Substitution of Val^{867}, the other large hydrophobic residue interacting with the C-terminal domain, impaired binding to the CaM mutants but not significantly to the wild type protein. The same result was obtained with the double mutant V866A/V867A as well as the charge reversal substitution R859E, indicating that substitutions in C-lobe contacts are critical once the "wraparound" configuration of CaM is disturbed by mutations in the EF-hands. Conversely, N-lobe anchor residue substitution did not abrogate mutant CaM binding (Fig. 6, *bottom panel*). GST-7A-C^{L876A} retained binding to both the N-terminal CaM 1,2 and C-terminal CaM 3,4 mutants but failed to detectably bind CaM 1–4. Individual side chain contributions to the interaction of GST-7A-C with the N-lobe of CaM were investigated by mutating Met^{872} to either alanine or glutamic acid and by introducing a proline in lieu of arginine Arg^{861} (Fig. 6, *bottom half*). M872A had no effect on binding to any of the CaM mutants except CaM 1–4 and, judging by band intensity, may even increase binding to CaM 1,2. In contrast, the M872E substitution reduced binding to all CaM constructs, including wild type CaM. This is in line with the uncharged nature of the side chains in CaM that lie close to

FIGURE 5. **Model of CaM interaction with the CaM-binding site of mGluR 7A.** The coordinates of the CaM homology model were used to calculate the molecular surface of the N- and C-terminal domains of CaM. *A,* cross-section through the surface (colored by atom type with carbon in *black*, oxygen in *red*, nitrogen in *blue*, and hydrogen in *white*), and mGluR 7A-(856–879) is depicted as a *ribbon* and *stick* representation colored similarly. *B,* model depicts the charged rim of CaM and the interactions made with the KRKR sequence of the mGluR 7A-(856–879), which is colored *green* for carbon for clarity. In both images mGluR 7A-(856–879) and CaM residues are listed in *italics* and *regular font*, respectively. The displays were created using MolMol (57). *C,* schematic diagram of the predicted interactions between mGluR 7A-C and the Ca^{2+}/CaM complex. The *line* represents the α-helical structure of mGluR 7A-(856–879). The principal interacting residues of the N- (*top*) and C-lobes (*bottom*) of CaM are *boxed* above and below the mGluR 7A peptide sequence. Predicted side chain interactions are indicated by *dashes*.

FIGURE 6. **Mutations of hydrophobic anchor residues in mGluR 7A-C differentially affect CaM binding.** Different GST-7A-C constructs carrying point mutations of charged and hydrophobic (labeled with *asterisks*) anchor residues were used in pulldown assays with GFP-tagged wild type (*WT*) or mutant CaM as presented in Fig. 1. Binding to the GST-7A-C wild type protein (*top*) and mutants relevant for C-lobe (*middle*) and N-lobe (*bottom*) interactions is shown. Ca^{2+} (300 μM) was present in all incubations. Note that GST-7A V867A still binds wild type CaM, but not CaM 1,2, whereas GST-7A F863A fails to bind both proteins. GST-7A M872A increases, and M872E and R861P decrease, binding to GFP-CaM 3,4. For further explanation, see text.

Met^{872} (see above and Fig. 5*C*). Mutation R861P had the most pronounced effect on CaM binding seen upon substitution of residues that interact with the N-lobe. This is consistent with this substitution both removing a long side-chain interaction with the N-lobe interface and perturbing the helical nature of the ligand. Taken together, the data highlight the importance of Phe^{863} and reinforce the observation that the mGluR 7A binds more strongly to the C-terminal domain than to the N-terminal domain of CaM.

DISCUSSION

In this study, we investigated how Ca^{2+}/CaM interacts with the cytoplasmic tail region of mGluR 7A, a low affinity G-protein-coupled glutamate receptor that mediates feedback inhibition at presynaptic transmitter release sites (4, 5, 11). Our first major result is that Ca^{2+}/CaM interacts with mGluR 7A-C primarily via its C-lobe. The observation that CaM 1,2 still bound tightly to mGluR 7A-C might indicate that this interaction represents another example of the "functional bipartition" of Ca^{2+}/CaM action, which has been discovered in Paramecium by Saimi and Kung (51). These authors found that mutations in the N-lobe of CaM disrupted Ca^{2+} activation of a potassium channel, whereas mutations in the C-lobe abolished Ca^{2+} activation of a sodium channel, thus revealing a potentially general mechanism through which Ca^{2+}/CaM could enrich its signaling repertoire. Some types of CaM-target interaction involve "pre-binding" by one of the lobes in the absence of Ca^{2+} or at very low Ca^{2+} concentrations, a process that accelerates Ca^{2+}/CaM actions triggered by rises in cytosolic Ca^{2+} levels. Such mechanism could be particularly important in presynaptic terminals, where Ca^{2+} influx triggered in the millisecond time range plays a crucial role in rapidly regulating neurotransmitter release and synaptic vesicle recycling (52).

Second, we employed a GFP-7A-C fusion protein to re-examine the stoichiometry of CaM binding by gel filtration. This approach clearly distinguishes 1:1 from higher order stoichiometries and allows the analysis of CaM-target complexes in protein extracts from mammalian cells as compared to studies with bacterial fusion proteins (53). Here, gel filtration of extracts prepared from GFP fusion protein-expressing cells did not show any size shifts larger than 20 kDa, suggesting that in our experiments only Ca^{2+}/CaM was recruited from the pool of endogenous proteins. Also, in 5 mM EGTA all mGluR 7A-C protein migrated as a homogeneous peak of ~38 kDa, consistent with the interaction being strictly Ca^{2+}-dependent. These results corroborate a 1:1 stoichiometry of the mGluR 7A-C-Ca^{2+}/CaM interaction using proteins expressed in mammalian cell extracts. Based on our results, a simultaneous interaction of Ca^{2+}/CaM with both C-tails of the dimeric receptor can be excluded.

Third, we employed high resolution NMR to define the molecular nature of the interaction between CaM and mGluR 7A using two peptides comprising residues Val^{856}–Arg^{875} and Val^{856}–Lys^{879} of the receptor's CaM binding region. Both peptides bound with high affinity to CaM. Comparison of the peptide-induced chemical shift perturbations of CaM allowed to define the orientation of the peptides within the Ca^{2+}/CaM·peptide complexes. The tumbling times of the individual domains in peptide-free and -bound CaM are consistent with a transition from an open to a closed CaM conformation. We examined the domain orientations of the CaM lobes in the peptide-bound state and found that CaM binds mGluR 7A in a wraparound structure, and that the binding region of mGluR 7A corresponds to a 1-8-14 CaM-binding motif.

By combining mutational analysis and molecular modeling, we have also been able to identify several mGluR 7A-C residues that are critical for CaM recognition. Based on our structural data, a homology model of the CaM-mGluR 7A binding peptide complex was built using the smMLCK-CaM complex as template. The importance of residues predicted to be required for Ca^{2+}/CaM binding was tested by binding assays with mutated GST-7A-C constructs. First, the three hydrophobic anchor residues of mGluR 7A-C that interact with the C-lobe of CaM were examined. Phe^{863}, a side chain positioned deeply in the hydrophobic pouch, was found to be essential for Ca^{2+}/CaM binding. The presence of Phe^{863} appeared to be sufficient for binding of wild type CaM, because binding still occurred when the neighboring hydrophobic residue Val^{867} or both Val^{866}/Val^{867} were mutated. The same mutants failed to bind CaM 1,2; apparently the Ca^{2+}-induced conformational change of the N-lobe has to "lock" the bound helix. Notably, whereas the sequences of mGluR 7 and mGluR 8 are identical throughout the CaM-binding motif, in mGluR 4 a leucine is found at the position of the

critical hydrophobic residue Phe^{863}. This substitution does not impair *in vitro* binding to wild type CaM (12), but it could be relevant for subtype-specific differences in the Ca^{2+}/CaM–mediated regulation of group III mGluRs. The substitution M872A increased CaM 1,2 binding, suggesting that introducing a smaller side chain facilitates other hydrophobic and charge interactions. Consistent with this view, replacement of Met^{872} by a larger, negatively charged residue (mutant M872E) caused a highly significant reduction in bound Ca^{2+}/CaM.

Ionic interactions contribute importantly to Ca^{2+}/CaM recruitment. Although positively charged amino acids preceding CaM binding domains are known to aid in orienting the binding helix on CaM by interacting with the negatively charged rim of the C-lobe, residues of mixed charges also have to be present on the N-lobe (50). Substitution of the positively charged residue Arg^{859} by an oppositely charged glutamate (R859E) was similar in its effect to mutation of the hydrophobic residues Val^{866} and Val^{867}, *e.g.* a loss of binding to CaM 1,2. Replacement of Arg^{861} by an uncharged residue (R861P) reduced binding to the N-lobe compared with M872A. However, introduction of a proline may disrupt the α-helical structure of mGluR 7A-C, and the reduced binding thus may not only reflect the loss of side-chain interactions. Here, we not only identified the basic side chains of mGluR 7A-C expected to interact with the C-lobe (Gln^{857}, Arg^{859}, and Lys^{860}), but we also found a set of purely basic interactions between mGluR 7A-C (Lys^{858}, Arg^{861}, and Lys^{864}) and the N-lobe of CaM (see Fig. 5). In previous experiments (12), we had been unable to dissect the contribution of the charged residues preceding the CaM binding region when using wild type CaM, and hence we concluded that the charged residues surrounding Phe^{863} are not important for CaM binding. The data presented here convincingly demonstrate that these charged residues are indeed crucial. Their precise roles are presently unclear but could lie in CaM binding prior to the Ca^{2+}-induced conformational change of the N-lobe.

The modeling results discussed above suggest that CaM binding might interfere with G$\beta\gamma$ binding via its N- and C-lobe interaction with residues Lys^{858}, Arg^{859}, and, less importantly, Gln^{857} of mGluR 7A-C (12). If only C-lobe activation were necessary to displace G$\beta\gamma$, modest changes in Ca^{2+} levels should be sufficient to cause displacement as compared with mechanisms that require activation of the N-lobe of CaM, which has a 10-fold lower Ca^{2+} binding affinity (54). Such N-lobe-dependent regulation has been found for P/Q-type Ca^{2+} channels (55), which are downstream targets in the mGluR 7/G$\beta\gamma$-pathway. Thus, Ca^{2+}/CaM could differentially regulate mGluR 7 and P/Q channels, because of differential C- or N-lobe activation in response to local changes of Ca^{2+}. This may provide an economic mechanism to temporally disperse different Ca^{2+} effects. Our model also explains how phosphorylation of serine 862 may inhibit CaM binding by inter-atomic repulsion. Ser^{862} is phosphorylated by several protein kinase (PK) isoforms *in vitro*, *e.g.* PKC (13, 24), PKA, and PKG (16). Activation of PKC has been shown to reduce inhibition of glutamate release by group III mGluRs at Schaffer collateral synapses in the CA1 region of the hippocampus (56). Notably, a GST-7A-C S862E construct mimicking phosphorylation has been shown not to bind Ca^{2+}/CaM, consistent with the approximate 1000-fold reduction of Ser(P)^{862}-mGluR 7A-(856–875) binding to CaM *in vitro* and differences in electrostatic potential controlling CaM binding (13).

In conclusion, our analysis of the structural determinants of Ca^{2+}/CaM binding to mGluR 7A-C refines our understanding of the mechanisms that control group III mGluR signaling via competition of intracellular proteins for receptor-binding sites. Our data are consistent with the proposal that these receptors act as key regulatory molecules in neurotransmitter release and epileptogenesis (8). The intriguing question of how activity-dependent changes in intracellular Ca^{2+} levels may fine-tune mGluR-mediated feedback inhibition is awaiting future structural and kinetic studies of C- and N-lobe binding to mGluR 7A-C. This is particularly important in face of the highly compartmentalized and very rapid kinetics of presynaptic Ca^{2+} influx (52).

Acknowledgments—We thank Drs. J. P. Adelman and S. Nakanishi for the generous supply of CaM mutant and mGluR cDNAs, respectively; A. Arends for expert technical assistance; and Maren Baier for secretarial help. We also thank the Wellcome Trust for funding of the NMR facility in Southampton (to J. M. W.) and the Medical Research Council for access to the National NMR Facility at Mill Hill.

REFERENCES

1. Nakanishi, S. (1994) *Neuron* **13,** 1031–1037
2. Pin, J. P., and Duvoisin, R. (1995) *Neuropharmacology* **34,** 1–26
3. Conn, P. J., and Pin, J. P. (1997) *Annu. Rev. Pharmacol. Toxicol.* **37,** 205–237
4. Nakanishi, S., Nakajima, Y., Masu, M., Ueda, Y., Nakahara, K., Watanabe, D., Yamaguchi, S., Kawabata, S., and Okada, M. (1998) *Brain Res. Brain Res. Rev.* **26,** 230–235
5. Dev, K. K., Nakanishi, S., and Henley, J. M. (2001) *Trends Pharmacol. Sci.* **22,** 355–361
6. Perroy, J., Prezeau, L., De Waard, M., Shigemoto, R., Bockaert, J., and Fagni, L. (2000) *J. Neurosci.* **20,** 7896–7904
7. Kinoshita, A., Shigemoto, R., Ohishi, H., van der Putten, H., and Mizuno, N. (1998) *J. Comp. Neurol.* **393,** 332–352
8. Sansig, G., Bushell, T. J., Clarke, V. R., Rozov, A., Burnashev, N., Portet, C., Gasparini, F., Schmutz, M., Klebs, K., Shigemoto, R., Flor, P. J., Kuhn, R., Knoepfel, T., Schroeder, M., Hampson, D. R., Collett, V. J., Zhang, C., Duvoisin, R. M., Collingridge, G. L., and van der Putten, H. (2001) *J. Neurosci.* **21,** 8734–8745
9. Callaerts-Vegh, Z., Beckers, T., Ball, S. M., Baeyens, F., Callaerts, P. F., Cryan, J. F., Molnar, E., and D'Hooge, R. (2006) *J. Neurosci.* **26,** 6573–6582
10. Welcome Trust Case Consortium (2007) *Nature* **447,** 661–678
11. El Far, O., and Betz, H. (2002) *Biochem. J.* **365,** 329–336
12. El Far, O., Bofill-Cardona, E., Airas, J. M., O'Connor, V., Boehm, S., Freissmuth, M., Nanoff, C., and Betz, H. (2001) *J. Biol. Chem.* **276,** 30662–30669
13. Airas, J. M., Betz, H., and El Far, O. (2001) *FEBS Lett.* **494,** 60–63
14. Rhoads, A. R., and Friedberg, F. (1997) *FASEB J.* **11,** 331–340
15. O'Connor, V., El Far, O., Bofill-Cardona, E., Nanoff, C., Freissmuth, M., Karschin, A., Airas, J. M., Betz, H., and Boehm, S. (1999) *Science* **286,** 1180–1184
16. Sorensen, S. D., Macek, T. A., Cai, Z., Saugstad, J. A., and Conn, P. J. (2002) *Mol. Pharmacol.* **61,** 1303–1312
17. Babu, Y. S., Sack, J. S., Greenhough, T. J., Bugg, C. E., Means, A. R., and Cook, W. J. (1985) *Nature* **315,** 37–40
18. Linse, S., and Forsen, S. (1995) *Adv. Second Messenger Phosphoprotein Res.* **30,** 89–151
19. Schumacher, M. A., Rivard, A. F., Bachinger, H. P., and Adelman, J. P.

(2001) *Nature* **410,** 1120–1124
20. Peterson, B. Z., DeMaria, C. D., Adelman, J. P., and Yue, D. T. (1999) *Neuron* **22,** 549–558
21. Mori, M. X., Erickson, M. G., and Yue, D. T. (2004) *Science* **304,** 432–435
22. Hoeflich, K. P., and Ikura, M. (2002) *Cell* **108,** 739–742
23. Kunishima, N., Shimada, Y., Tsuji, Y., Sato, T., Yamamoto, M., Kumasaka, T., Nakanishi, S., Jingami, H., and Morikawa, K. (2000) *Nature* **407,** 971–977
24. Nakajima, Y., Yamamoto, T., Nakayama, T., and Nakanishi, S. (1999) *J. Biol. Chem.* **274,** 27573–27577
25. Dev, K. K., Nakajima, Y., Kitano, J., Braithwaite, S. P., Henley, J. M., and Nakanishi, S. (2000) *J. Neurosci.* **20,** 7252–7257
26. Keen, J. E., Khawaled, R., Farrens, D. L., Neelands, T., Rivard, A., Bond, C. T., Janowsky, A., Fakler, B., Adelman, J. P., and Maylie, J. (1999) *J. Neurosci.* **19,** 8830–8838
27. Cook, A. G., Johnson, L. N., and McDonnell, J. M. (2005) *FEBS J.* **272,** 1511–1522
28. Kay, L. E., Xu, G. Y., and Yamazaki, T. (1994) *J. Magn. Reson.* **109,** 129–133
29. Wittekind, M., and Mueller, L. (1993) *J. Magn. Reson.* **101,** 201–205
30. Grzesiek, S., and Bax, A. (1992) *J. Am Chem. Soc.* **114,** 6291–6293
31. Rooney, L. M., Sachchidanand, and Werner, J. M. (2004) *Methods Mol. Biol.* **278,** 123–138
32. Ottiger, M., Delaglio, F., and Bax, A. (1998) *J. Magn. Reson.* **131,** 373–378
33. Cornilescu, G., Marquardt, J. L., Ottiger, M., and Bax, A. (1998) *J. Am Chem. Soc.* **120,** 6836–6837
34. Kay, L. E., Nicholson, L. K., Delaglio, F., Bax, A., and Torchia, D. A. (1992) *J. Magn. Reson.* **97,** 359–375
35. Farrow, N. A., Muhandiram, R., Singer, A. U., Pascal, S. M., Kay, C. M., Gish, G., Shoelson, S. E., Pawson, T., Formankay, J. D., and Kay, L. E. (1994) *Biochemistry* **33,** 5984–6003
36. Delaglio, F., Grzesiek, S., Vuister, G. W., Zhu, G., Pfeifer, J., and Bax, A. (1995) *J. Biomol. NMR* **6,** 277–293
37. Johnson, B. A., and Blevins, R. A. (1994) *J. Biomol. NMR* **4,** 603–614
38. Dosset, P., Hus, J. C., Marion, D., and Blackledge, M. (2001) *J. Biomol. NMR* **20,** 223–231
39. Dauber-Osguthorpe, P., Roberts, V. A., Osguthorpe, D. J., Wolff, J., Genest, M., and Hagler, A. T. (1988) *Proteins* **4,** 31–47
40. Geiser, J. R., van Tuinen, D., Brockerhoff, S. E., Neff, M. M., and Davis, T. N. (1991) *Cell* **65,** 949–959
41. Xia, X. M., Fakler, B., Rivard, A., Wayman, G., Johnson-Pais, T., Keen, J. E., Ishii, T., Hirschberg, B., Bond, C. T., Lutsenko, S., Maylie, J., and Adelman, J. P. (1998) *Nature* **395,** 503–507
42. Wall, M. E., Clarage, J. B., and Phillips, G. N. (1997) *Structure* (*Lond.*) **5,** 1599–1612
43. Meador, W. E., Means, A. R., and Quiocho, F. A. (1992) *Science* **257,** 1251–1255
44. Barbato, G., Ikura, M., Kay, L. E., Pastor, R. W., and Bax, A. (1992) *Biochemistry* **31,** 5269–5278
45. Meador, W. E., Means, A. R., and Quiocho, F. A. (1993) *Science* **262,** 1718–1721
46. Osawa, M., Tokumitsu, H., Swindells, M. B., Kurihara, H., Orita, M., Shibanuma, T., Furuya, T., and Ikura, M. (1999) *Nat. Struct. Biol.* **6,** 819–824
47. Contessa, G. M., Orsale, M., Melino, S., Torre, V., Paci, M., Desideri, A., and Cicero, D. O. (2005) *J. Biomol. NMR* **31,** 185–199
48. Mal, T. K., Skrynnikov, N. R., Yap, K. L., Kay, L. E., and Ikura, M. (2002) *Biochemistry* **41,** 12899–12906
49. Ikura, M., Clore, G. M., Gronenborn, A. M., Zhu, G., Klee, C. B., and Bax, A. (1992) *Science* **256,** 632–638
50. Vetter, S. W., and Leclerc, E. (2003) *Eur. J. Biochem.* **270,** 404–414
51. Saimi, Y., and Kung, C. (1994) *FEBS Lett.* **350,** 155–158
52. Schneggenburger, R., and Neher, E. (2005) *Curr. Opin. Neurobiol.* **15,** 266–274
53. Kim, J., Ghosh, S., Nunziato, D. A., and Pitt, G. S. (2004) *Neuron* **41,** 745–754
54. Potter, J. D., Strang-Brown, P., Walker, P. L., and Iida, S. (1983) *Methods Enzymol.* **102,** 135–143
55. DeMaria, C. D., Soong, T. W., Alseikhan, B. A., Alvania, R. S., and Yue, D. T. (2001) *Nature* **411,** 484–489
56. Macek, T. A., Schaffhauser, H., and Conn, P. J. (1998) *J. Neurosci.* **18,** 6138–6146
57. Koradi, R., Billeter, M., and Wuthrich, K. (1996) *J. Mol. Graphics* **14,** 51–55